Acta Crystallographica Section B
Structural Science
ISSN 0108-7681

Crystal chemistry of orthosilicates and their analogs: the classification by topological types of suprapolyhedral structural units

G. D. Ilyushin,[a]* V. A. Blatov[b] and Yu. A. Zakutkin[b]

[a]Institute of Crystallography of RAS, Leninsky Pr. 59, Moscow 117333, Russia, and [b]Samara State University, Ac. Pavlov St. 1, Samara 443011, Russia

Correspondence e-mail: ilyushin@ns.crys.ras.ru

Received 13 June 2002
Accepted 20 August 2002

A method is developed for the analysis and classification of orthosilicates and their analogs $M_x(TO_4)_y$ containing M cations and tetrahedral TO_4 anions. The method uses the concepts of coordination sequence and crystal structure 'reduced' graphs and is optimized for orthostructures of any complexity. First, the suprapolyhedral level of crystal structure organization was studied, where T tetrahedra were considered as templates for condensing M polyhedra, constructing as a result T polyhedral microensembles. Using this methodology, the crystal structures of 54 orthosilicates and orthogermanates were analyzed within the first 12 coordination spheres of T nodes and were arranged into 21 topological types. The topological types were expanded with the analogs found within the orthostructures of phosphates, sulfates *etc.* T polyhedral microensembles were used for the topological classification of reconstruction mechanisms of thermal and baric phase transitions of orthosilicates.

1. Introduction

Historically the problem of silicate classification was first considered within structural mineralogy. Machatschki (1928) and Bragg (1930) proposed a classification scheme for silicate minerals based on the geometrical configuration of anionic Si-containing anions. Bragg (1930) assumed that all other structure components, except tetrahedrally coordinated Al atoms, played the role of cation-compensators of Si-containing anion charge. He arranged 25 silicate minerals with relatively simple chemical compositions and crystal structures into five groups according to dimensionality for nine types of silicon-containing radicals:

(i) orthotetrahedra $[SiO_4]^{4-}$;

(ii) self-contained groups $[Si_2O_7]^{6-}$, $[Si_3O_9]^{6-}$, $[Si_4O_{12}]^{8-}$, $[Si_6O_{18}]^{12-}$;

(iii) silicon–oxygen chains $[SiO_3]^{2-}$, $[Si_4O_{11}]^{6-}$;

(iv) silicon–oxygen sheets $[Si_2O_5]^{2-}$;

(v) silica-like networks, with the ratio represented by (Si, Al):O = 1:2.

This classification was based on the assumption that SiO_4 tetrahedra act as fundamental building 'bricks' of silicate crystal structures. Later Bragg's classification scheme was expanded to include newly discovered crystal structures and Si-containing anions (Schiebold, 1932, 1933; Hassel, 1934; Liebau, 1956, 1985; Zoltai, 1960; Bragg & Claringbull, 1965; Puschcharovskii, 1986; Bokij, 1984, 1998).

Liebau (1985) selected about 60 topologically different Si-containing anions. His classification excludes the following silicate classes: (i) containing Si atoms with coordination number CN = 6; (ii) with mixed silicon coordination (CN = 4 and 6); (iii) with edge condensation of Si tetrahedra; (iv) so-

called monosilicates (160 phases with orthotetrahedra and 90 phases with diorthotetrahedra); and (v) phases with mixed types of Si-containing anions. Other silicates are at present classified with seven Liebau parameters: (i) silicon CN, (ii) linkedness, (iii) branchedness, (iv) dimensionality, (v) multiplicity, (vi) chain and ring periodicity of silicate anions, and (vii) the number of topologically different Si anions. The distribution of the types of Si-containing anions is extremely nonuniform: 160 and 90 silicates (19 and 11% out of 856 crystal structures with one type of Si-containing anion) are orthosilicates and diorthosilicates, respectively, comprising 0D-groups $[SiO_4]$ and $[Si_2O_7]$. Isolated instances are found for 41 Si-containing anions (for example, short chains $[Si_5O_{16}]^{12-}$).

There is a 'chemical' reconstruction of Bragg's scheme (Puschcharovskii, 1986) where Si-containing anions are arranged into 21 groups according to the increase of stoichiometric ratio Si:O from 1:4 to 1:2. For instance, in this case, all 17 types of chain and ring radicals fall into the same SiO_3 group. Puschcharovskii (1986) also used this scheme for the classification of germanates and phosphates (ten groups in both cases).

Recently, Grice *et al.* (1999) applied Bragg's approach to classify borate minerals by 25 different isolated borate radicals consisting of BO_3 triangles and BO_4 tetrahedra. As a result, 168 borate crystal structures were arranged into 114 types.

The necessity of developing a more clearly differentiated variant of Bragg's scheme was noted by Zoltai (1960) and Liebau (1985). All further efforts to improve Bragg's scheme took into account additional primary building units (PBUs) forming silicate crystal structures. Liebau (1985) assumed silicates to be constructed with both silicon–oxygen and *M*-cation–oxygen polyhedra. Thus, in this scheme, the structure-forming roles of both *M* polyhedra and *T* tetrahedra are considered; moreover, this role is assumed to increase with decreasing coordination number and increasing *M*-cation charge. At the same time, Liebau (1985) noted that such a classification would be too complex and practically senseless.

There are two special crystal structure models of silicates and phosphates containing *M* octahedra. Kostov (1971) considered infinite chains, ribbons or layers consisting of only *M* octahedra as the 'structural foundations' of such silicate minerals. Moore (1984) developed a similar structural classification for phosphate minerals (mainly orthophosphates). Belov (1965) proposed a more detailed differentiation of silicate structures selecting a group of silicates with large *M* cations and assuming building blocks of commensurate fragments like Ca octahedra and diorthogroup Si_2O_7.

At present, the most typical variants of silicate crystal structure organization have been classified using the structure-type concept, and the most frequent invariant polyhedral fragments (ensembles) have been selected. These were discussed in detail by Smith (1988) for zeolite-like aluminosilicates (where the PBUs are AlO_4 and SiO_4 tetrahedra), by Ilyushin & Demianets (1989, 2001) for zirconogermanates and their analogs [where the PBUs are MO_6 octahedra (M = Zr, Hf, Ti, Sn) and GeO_4 tetrahedra], and by Ilyushin & Blatov (2002) for zirconosilicates and their analogs (where the PBUs are MO_6 octahedra and SiO_4 tetrahedra).

Let us emphasize that formally selected condensed Si-containing anions are, in general, not products of simultaneous polymerization of primary polyhedral particles (SiO_4 tetrahedra). There are only five such polymerization instances; they are realized in the polymorphous phases of silicon dioxide. In their crystal structures, the cluster precursors, consisting of SiO_4 tetrahedra, form simultaneously (with no participation of other atoms) the structure types of cristobalite, tridimite, quartz, coesite and keatite using a self-assembling mechanism (Ilyushin & Demianets, 2001, 2002). The *T* radicals mentioned above have no mutual structural–genetic relations and reflect merely the last stage of evolution of the cluster precursors, which already contain all chemically significant structural components (in particular, *T* tetrahedra) at the first stages of crystal structure formation (Ilyushin & Demianets, 1989, 2001). Thus, the topological type of the condensed Si-containing anion can be used as an initial classification parameter to select a subgroup of topologically similar or equal compounds within the silicate group, because in this case all structural components are significant for classification.

Let us enumerate the principal problems that have not yet been resolved within Bragg's classification scheme:

(i) *The problem of hierarchy and unambiguity*. In the modern form of Bragg's classification by *T* radicals, all silicates are arranged in 60 extremely unequal groups, but further arrangement within each group has not been performed (see classification schemes of Liebau, 1985; Puschcharovskii, 1986; Bokij, 1998; Grice *et al.*, 1999).

(ii) *The problem of comparing*. Silicates have different chemical-complexity ranks R = 3–8 (the number of chemically different atoms) and their direct comparison yields little crystallochemical information, even if Si-containing anions are the same in their crystal structures. To compare them with each other one should select the rank-equivalent *substructures* (Ilyushin & Blatov, 2002). Structures or substructures of the same rank can be compared as follows:

(*a*) chemically different silicates with the same stoichiometric composition (for instance, the non-isostructural pairs Li_4SiO_4 and Na_4SiO_4 with R = 3 or Na_2ZrSiO_5 and Na_2TiSiO_5 with R = 4);

(*b*) chemically equivalent silicates (comprising equal sets of chemical elements) with different stoichiometric composition, *i.e.* the phases obtained in the same silicate system.

In the first case, we can study morphotropic series and possible phase transitions; the second case reveals structural–genetic relations in the system. In this respect, the orthosilicates can be classified only within the families of ternary compounds M—Si—O (R = 3), quaternary compounds $M1$—$M2$—Si—O (R = 4) *etc.*

(iii) *The problem of completeness*. In the most complete modern silicate systematics (Bokij, 1998), minerals are arranged using Bragg's scheme only, whereas numerous synthetic silicates are forgotten.

(iv) *The problem of exceptions*. Following Bragg (1930), aluminosilicates (zeolites and feldspars) have to fall into a

special branch of 'three-dimensional tetrahedral SiO_2-like crystal structures'. In this case, the classification scheme performs an improper function: it determines the constructing role of chemically different SiO_4 and AlO_4 groups giving no comparison criteria except their geometrical similarity. In this connection, Zoltai (1960), Wells (1985), Liebau (1985) and Bokij (1998) attempted to expand the list of *T* elements (Li, Be, B *etc.*) that can compose *T* radicals along with silicon. On the other hand, Bokij (1998) considered no silicate minerals comprising non-metal atoms, for instance, eulytite $Bi_4(SiO_4)_3$ and other Bi-containing silicates, since Bi^{3+} ions are not compensators of Si anions in Bragg's model.

In this respect, the goals of the present study are as follows:

(i) to investigate the principles of silicate crystal structure organization on the suprapolyhedral level (Ilyushin & Blatov, 2002), where all structure elements are connected by hierarchical geometrical–topological relations;

(ii) to search for ways of overcoming the aforementioned problems of Bragg's classification scheme using modern methods of crystallochemical analysis to be described in §§3 and 4.

As investigation objects, we use a large family of simple orthosilicates and a chemically and structurally related orthogermanate family (Table 1) because they have not yet been classified in detail. These families were expanded with analogs found among orthophosphates, sulfates and other orthophases during the investigation.

2. Orthostructures: a traditional view

The orthotetrahedral phases, silicates and germanates $M_x(TO_4)_y$, contain invariant PBUs (SiO_4 and GeO_4 tetrahedra) and relate to the systems with the smallest rank $R = 3$. In the 54 phases considered, all O atoms belong to *T* tetrahedra. Hereinafter, we shall call these compounds *orthostructures* or *orthophases*, thereby separating them from the phases containing additional O atoms together with *T* tetrahedra, which are considered no further in this study. An orthostructure can be traditionally described by one of the following models:

(i) *Bragg's model*. Within the atomic polyhedral model, one should represent an

Table 1
Distribution of simple orthosilicates and orthogermanates $M_y(XO_4)_z$ with topological and structure types.

No. of compound	Topological type: No.	Name†	Compound	Mineral or polymorphous form	Space group	CC‡
M(+1)						
1	1	ORSi-1	Li_4SiO_4	Synthetic	$P2_1/m$	8222
2	2	ORGe-1	Li_4GeO_4	Synthetic	*Cmcm*	65177
3	3	ORSi-2	Na_4SiO_4	Synthetic	$P\bar{1}$	62594
4			K_4GeO_4	Synthetic		37271
5			Na_4GeO_4	Synthetic		62595
6	4	ORSi-3	K_4SiO_4	Synthetic	$P2_1/c$	66073
7	5	ORGe-2	Ag_4GeO_4	Synthetic	$P\bar{1}$	78803
8	6	ORGe-3	Ag_5GeO_4	Synthetic	$P2_1/n$	71897
M(+2)						
9	7	OLI	Ca_2SiO_4	γ-phase	*Pbnm*	82995
10			Co_2SiO_4	Olivine	*Pbnm*	50072
11			Fe_2SiO_4	Fayalite	*Pbnm*	54034
12			Mg_2SiO_4	Forsterite	*Pbnm*	30958
13			Mn_2SiO_4	α-tephroite	*Pbnm*	26376
14			Ni_2SiO_4	Liebenbergite	*Pbnm*	100644
15			Cd_2GeO_4	Synthetic	*Pmcn*	20873
16			Mg_2GeO_4	Synthetic	*Pnma*	63533
17			Mn_2GeO_4	Synthetic	*Pnma*	23587
18	8	ORSi-4	Cr_2SiO_4	Synthetic	*Fddd*	75639
19			Cd_2SiO_4	Synthetic		23943
20			Hg_2GeO_4	Synthetic		26340
21	9	SPI	Co_2SiO_4	Synthetic	$Fd\bar{3}m$	859
22			Fe_2SiO_4	Synthetic		87462
23			Ni_2SiO_4	Synthetic		200129
24			Co_2GeO_4	Synthetic		29348
25			Mg_2GeO_4	Synthetic		1086
26			Ni_2GeO_4	Synthetic		69508
27			Cu_2GeO_4	Synthetic	$I4_1/amd$	100796
28	10	PHE	Be_2SiO_4	Phenakite	$R\bar{3}$	83726
29			Zn_2SiO_4	Willemite		200433
30			Zn_2GeO_4	Synthetic		68382
31	11	WIL-HP	Zn_2SiO_4	Willemite-HP	$I\bar{4}2d$	9147
32	12	ORSi-5	Ca_2SiO_4	α-phase	$Pna2_1$	82996
33	13	LAR	Ca_2SiO_4	β-larnite	$P2_1/n$	79551
34	14	ORSi-6	Eu_2SiO_4	Synthetic	$P2_1/c$	23615
35			Sr_2SiO_4	β-phase	$P2_1/n$	36041
36	15	ORSi-7	Ba_2SiO_4	Synthetic	*Pmcn*	6246
37			Eu_2SiO_4	β-phase	*Pnma*	1510
38	16	ORGe-4	Sr_2GeO_4	α-phase	$Pbn2_1$	83345
M(+2), *M*(+3)						
39	17	GAR	$Fe_5(SiO_4)_3$	Garnet	$Ia\bar{3}d$	27377
40			$Mn_5(SiO_4)_3$			27382
M(+3)						
41	18	EUL	$Bi_4(SiO_4)_3$	Eulytite	$I\bar{4}3d$	402349
42			$Bi_4(GeO_4)_3$	Synthetic		39231
M(+4)						
43	19	ZIR	$ZrSiO_4$	Zircon	$I4_1/amd$	71943
44			$HfSiO_4$	Hafnon		59111
45			$ThSiO_4$	Thorite		1615
46			$USiO_4$	Coffinite		15484
47			$ThGeO_4$	Synthetic		202082
48	20	HUT	$ThSiO_4$	Huttonite	$P2_1/n$	1614
49	21	SHE	$ZrGeO_4$	Synthetic (scheelite)	$I4_1/a$	29262
50			$HfGeO_4$	Synthetic		202080
51			$ThGeO_4$	Synthetic		202081
52			$UGeO_4$	Synthetic		16639
53			$CeGeO_4$	Synthetic		PDF 40-1182
54			$ZrSiO_4$-HP	Synthetic		Kusaba *et al.* (1986)

† Each topological family (topological type containing more than one compound) is assigned the contracted name of a mineral phase or of a well known isostructural analog. If the topological family or type contains no minerals it is assigned standard enumerated abbreviations ORSi or ORGe for the families comprising orthosilicates (and, probably, orthogermanates) or only orthogermanates, respectively. ‡ Collection codes of compounds in the ICSD are given.

orthostructure as a packing of TO_4 tetrahedra surrounded by M atoms (Fig. 1*a*). This is the simplest model, and it cannot be used for detailed systematics of orthosilicate crystal structures owing to the lack of additional criteria characterizing the structure as a whole.

(ii) *Pauling's model*. It is assumed that any crystal structure can be represented by an array of interconnected coordination polyhedra of all T and M atoms (Fig. 1*b*). The types of M polyhedra to be distinguished by geometrical properties and chemical composition can serve as additional structure criteria for a more differentiated arrangement of silicates. However, in complex cases, typical for silicates, when the number of types of M polyhedra can reach 3–5 or sometimes greater values, such an approach also meets difficulties. It remains unclear what types of M polyhedra are significant for classification.

(iii) *Wells's model*. As a three-dimensional periodic atomic array, an orthostructure can be represented within the topological model (Wells, 1977) as a non-oriented graph where atoms and interatomic bonds correspond to graph vertices (nodes) and edges, respectively. The crystal structure is determined by the connectivity degree of the vertices as, for instance, a 4,6-connected net for olivine or spinel or a 4,8-connected net for zircon or scheelite. The problem with this model is the rational selection of nodes to use as additional classification criteria, taking into account their physical meaning as real atomic polyhedral or polyhedral structural ensembles.

(iv) *Close O-packing model*. Bragg (1930), having only considered silicates constructed of T tetrahedra and M octahedra, assumed that it was only in these cases that both M octahedra and T tetrahedra played an important structure-forming role. These two types of polyhedra are the most frequent PBUs in silicate minerals, and their condensation often results in geometrically close packings of O atoms (O-packings). Bragg (1930) found locally regular O-packings in a number of silicates, but he noted that some investigators arrogated to him the hypothesis that all silicates should be considered as close O-packings, probably with some extra O atoms. In fact, locally regular O-packings as tetrahedral or octahedral groups give globally close O-packings in few cases.

However, in the modern crystal chemistry of silicates (Wells, 1985), the model of close O-packing (distorted to some extent) with electropositive atoms allocated in its voids remains rather widespread. Moreover, Wells (1985) contended that T radicals are not necessarily the main architectural elements of silicates.

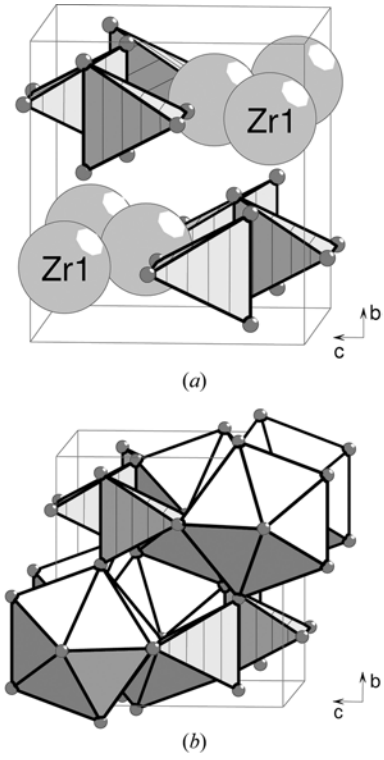

Figure 1
Zircon crystal structure according to (*a*) Bragg and (*b*) Pauling.

3. Methods of crystal structure classification using coordination sequences

Using Wells's model, Meier & Moeck (1979) proposed the classification of zeolites by *coordination sequence* (CS) $\{N_k\}$ (Brunner & Laves, 1971) for *connected substructures*[1] of T atoms; CSs were calculated within the first five coordination spheres ($k = 1$–m, $m = 5$). Moreover, Meier & Moeck (1979) used CSs of crystallographically different T atoms in a given framework to test their topological equivalence: CS equality indicated an additional 'topological' symmetry of the framework. This study stimulated a number of investigations of CSs for T atoms in zeolite frameworks (Stixrude & Bukowinski, 1990; O'Keeffe, 1995; Grosse-Kunstleve *et al.*, 1996). At present, such CSs are accepted as significant topological zeolite characteristics and are calculated up to $m = 10$ (Meier *et al.*, 1996).

The advantages of using CSs for the classification of framework compounds of any composition and structure include the following:

(i) the unambiguous and not too laborious calculation of CS;

(ii) the simplicity of comparing the CS sets for framework-forming atoms while classifying;

(iii) the possibility of combining local and global approaches to the description of crystal structure: though, strictly speaking, CS is determined for a finite structural fragment, in practice the equality of $\{N_k\}$ sets for corresponding framework-forming atoms of compared substructures within the first 3–5 coordination spheres indicates global isomorphism (Blatov, 2000).

The method of coordination sequences was used by Blatov (2000) to develop a novel scheme of crystallochemical analysis and classification, where the crystal structure as a whole is represented by a finite 'reduced' graph that contains information on the whole system of interatomic bonds.

[1] A connected substructure is a subset of net nodes keeping connectivity between them. All the net nodes not belonging to this subset are to be contracted to the subset nodes (Ilyushin & Blatov, 2002).

Isomorphism of 'reduced' graphs of the frameworks to be compared indicates their topological equivalence and that they fall into the same *topological type* or *topological family*.

According to Blatov (2000) and Ilyushin & Blatov (2002), we shall use the following basic topological representations of orthostructures:

(i) as a net, when the orthostructure is characterized by the whole net of interatomic bonds and assumes no simplification based, for instance, on the bond-type differences;

(ii) as a set of multiatomic (polyhedral) structure units, each of which is to be analyzed as a single whole, without taking into account its internal structure. In particular, such classification models are used for framework zeolites while representing them as connected T sublattices (with contracted O atoms of T tetrahedra).

Finally, topological equivalence of representations of a pair of crystal structures can be determined by comparing CSs for all atoms composing substructures that correspond to these representations. One should take into account the possibility of topological symmetry of crystallographically non-equivalent atoms following from equality of their $\{N_k\}$ sets. In this case, topologically symmetrical atoms belong to the same topological sort (Blatov, 2000).

4. Levels of structure organization of *MT* orthophases

The topological method of using coordination sequences to give strict classification criteria as sets of topological indices does not consider explicitly how the restrictions caused by chemical composition, and by geometrical features of M and T PBUs, influence the crystal structure's topological properties. Following Ilyushin & Blatov (2002), let us consider the combined analysis of topological and geometrical properties of MT orthostructures on the three levels of their structure organization: atomic, polyhedral and suprapolyhedral.

At the *atomic* level, the main classification parameters are the characteristics of point models of MT orthostructures: the number and symmetry of occupied Wyckoff positions, and stoichiometric ratios for M, T and O atoms. In general, MT orthostructures are described by the $M_aT_bO_c$ formula, with $c/b = 4$. Thus, all chemical formulae of oxygen-containing orthophases can be obtained by enumerating the oxidation states of M atoms (for T atoms oxidation state $\xi_T = 4$) for a and b interacting hypothetical polyhedral particles,

$$a[M(z+)(OH)_z] + b[T(4+)(OH)_4], \qquad (1)$$

by their full oxidation up to M_pTO_4 ($p = a/b$; $z = 4/p$). Because of the limited range of oxidation states of M atoms ($\xi_M = 1$–4) in orthosilicates and orthogermanates, p can be equal only to 4, 2, 4/3 or 1, and the chemical composition of orthostructures varies in the series M_4TO_4–M_2TO_4–$M_4T_3O_{12}$–MTO_4.

At the *polyhedral* level, one should first identify MO_n polyhedra and TO_4 tetrahedra and should then determine their role as framework-forming PBUs. At this step, a chemical compound is to be related to the class of MT orthostructures.

At the *suprapolyhedral* level, MT frameworks should be classified by atomic coordination polyhedra, and oligomeric structural units consisting of several PBUs should be selected. Such polyhedral ensembles are *suprapolyhedral invariants* of the topological type (family) to which the orthostructure has been related. Using them, one can search for representatives of this family in other classes of orthostructures (phosphates, sulfates *etc.*). Orthophases can have different space groups, lattice parameters, and degrees of geometrical distortion of M and T polyhedra, but the structure connectedness reflected by coordination sequences or by a suprapolyhedral invariant remains the same.

We have used the following algorithm for hierarchically constructing suprapolyhedral invariants (Ilyushin & Blatov, 2002).

First sublevel. For each of the crystallographically non-equivalent MO_n and TO_4 polyhedra, all the polyhedra directly connected with them are taken into account; suprapolyhedral invariants of only two compositions are possible:

(i) $[MO_n]$–$\{[MO_n]_i, [TO_4]_j\}$, since M polyhedra can have contacts with each other;

(ii) $[TO_4]$–$\{[MO_n]_i\}$; according to the orthostructure definition there are no TO_4–TO_4 contacts.

Thus, at the first sublevel, suprapolyhedral invariants are *polyhedral microensembles* (PMEs) (Ilyushin & Blatov, 2002) constructed with M and T polyhedra; their geometrical view is unambiguously determined by the set of i and j indices. After the PME construction, it is important to determine topological non-equivalence of M and T nodes as was mentioned above. The following questions have a special meaning while classifying MT orthostructures with CSs: what is the minimum number of M and/or T nodes from which all the frameworks considered can be constructed, and how many CSs and types of nodes are required to identify a framework unambiguously? Thus, at this sublevel, the set of CSs for the framework atoms becomes the most important classification criterion.

Second and higher sublevels. For each PME of the first sublevel (PME-1), all PBUs are to be considered that are connected with M and T polyhedra of PME-1. As a result, a PME of the second sublevel (PME-2) is formed. More complex PMEs of the third, fourth *etc.* sublevels may be similarly generated from the PMEs of lower sublevels. Following a previous study (Ilyushin & Blatov, 2002), we shall not go beyond the first sublevel of the structural–topological analysis and shall consider only PME-1, hereafter referred to as PME.

PMEs help us visualize CSs for M and T nodes and, at the appropriate depth of calculation, reflect the connectedness of crystal-forming MT precursors and their space correlations. In the case of orthostructures, the $\{N_k\}$ set for any atom gives the number of cations and anions in its coordination spheres; odd and even k values correspond to anions (O atoms) and cations, respectively. Namely, the composition of a T PME in an oxo-orthostructure can be coded as follows: $\{ON_1, MN_2, ON_3, (M+T)N_4, ON_5, \ldots\}$, where $N_1, N_2, \ldots$ are the coordination-sequence numbers; O, M and T are atomic symbols.

Table 2
Coordination sequences for the first 12 coordination spheres of T atoms for the topological types of simple orthosilicates and orthogermanates.

			Coordination sequences $\{N_k\}$ (k = 1–12)											
Topological type	n	T atom	1	2	3	4	5	6	7	8	9	10	11	12
ZIR	8	Si(1)†	4	6	36	34	92	62	180	122	300	182	444	266
HUT	9	Si(1)†	4	7	42	42	126	94	251	167	420	266	630	379
PHE	4	Si(1)	4	8	21	28	57	62	111	108	181	168	270	242
WIL-HP	4	Si(1)	4	8	24	32	64	70	128	128	216	204	332	298
EUL	6	Si(1)	4	8	32	32	80	72	168	138	288	208	432	304
SHE	8	Ge(1)	4	8	44	42	112	84	228	150	376	240	568	342
OLI	6	Si(1)†	4	9	31	46	90	99	188	196	335	305	502	464
ORSi-4	6	Si(1)†	4	10	32	46	96	106	192	186	316	294	468	418
GAR	6, 8	Si(1)†	4	10	40	46	96	94	216	194	352	290	568	470
LAR	7, 8	Si(1)†	4	11	42	60	128	146	273	278	492	460	741	668
ORGe-4	6, 8, 9	Ge(1)†	4	11	41	60	131	153	301	311	578	557	949	869
		Ge(2)†	4	11	44	67	153	177	352	359	645	617	1016	923
ORSi-6	8	Si(1)†	4	11	43	62	138	161	312	317	564	532	868	782
ORSi-5	7–9	Si(3)†	4	11	41	62	144	170	347	359	649	613	1023	925
		Si(1)†‡	4	11	43	63	141	165	341	357	637	605	1009	911
		Si(2)†	4	11	46	70	159	185	356	361	655	618	1029	931
ORSi-7	9, 10	Si(1)†‡	4	11	49	74	178	199	398	397	732	669	1111	991
SPI	6	Si(1)	4	12	36	44	88	102	184	176	300	288	460	398
ORGe-3	2–4	Ge(1)†	4	14	19	41	45	99	90	165	145	269	212	367
ORGe-2	3–6	Ge(1)†	4	14	23	49	66	119	133	224	232	355	344	503
		Ge(2)†	4	14	28	56	66	119	135	224	234	360	346	513
ORSi-3	4–6	Si(1)†	4	14	28	64	90	170	204	334	355	549	545	805
ORSi-1	4–6	Si(5)†	4	14	26	56	70	129	142	232	239	367	367	538
		Si(3)†	4	15	27	55	75	137	155	248	247	391	379	560
		Si(7)†	4	15	27	58	73	132	150	241	239	379	360	533
		Si(1)†	4	15	28	58	73	135	154	249	259	408	398	586
		Si(4)†	4	15	28	58	73	137	149	237	242	378	383	568
		Si(6)†	4	15	28	60	75	139	153	251	262	410	406	593
		Si(2)†	4	15	28	60	75	139	157	254	263	414	399	584
ORSi-2	4–6	Si(1)†	4	15	29	64	88	161	186	304	319	488	475	708
ORGe-1	4	Ge(1)	4	16	26	48	66	126	136	214	222	352	328	470

† There are edge T–M contacts in this PME. ‡ There are face-to-face T–M contacts in this PME.

Unlike in the case of framework zirconosilicates (Ilyushin & Blatov, 2002), T (not M) nodes are the most useful for the classification of orthostructures because these nodes possess the following important properties:

(i) There are fewer crystallographically different T nodes than M and O nodes, which means a minimum density of T nodes in MTO nets; conversely, in zirconosilicates, M (not T) nodes have such a property.

(ii) The third coordination spheres of T atoms contain only M atoms.

In this respect, let us consider some features of topological analysis of T PMEs.

5. Experimental

Comparative analysis and classification of frameworks were performed with the program package *TOPOS* 3.2 (Blatov *et al.*, 2000) modified to support the methods described in §§3 and 4. The algorithm of investigation comprised the following steps:

(i) Creating a database of silicates and germanates with the rank $R = 3$. At this step, all chemically and/or crystallographically different compounds containing non-disordered Si and O atoms (585 phases) or Ge and O atoms (218 phases) were taken from the ICSD (Inorganic Crystal Structure Database; release 2001/1).

(ii) Calculating the adjacent matrix and searching for PBUs for each crystal structure using the program *AutoCN* (Blatov *et al.*, 2000). According to Blatov & Serezhkin (2000), this only takes into account the strong cation–anion contacts, which correspond to the 'major' faces[2] of atomic Voronoi–Dirichlet polyhedra with solid angles $\Omega > 5\%$ of the total solid angle 4π. The adjacent matrices were constructed by the method of spherical sectors using the Slater system of atomic radii.

(iii) Calculating $\{N_k\}$ sets for all possible crystal structure representations and comparing their topological properties using the program *IsoTest* (Blatov, 2000), namely:

(*a*) selecting orthostructures using the condition $\{N_k\} = \{4, 0, 0, \ldots\}$ for the subnet $\{T, \mathrm{O}\}$ where T atoms have bonds with and only with four O atoms and each of these O atoms has no bonds with other T atoms;

(*b*) comparing topological properties of the nets $\{M, T, \mathrm{O}\}$ in the orthostructures selected; forming topological families and topological types (Table 2).

At this step, 54 orthostructures of silicates and germanates were found (Table 1).

(iv) Topological comparison of orthosilicate and orthogermanate crystal structures with binary and ternary compounds. The databases created with the program *IsoTest* were used, which contained 1134 topological types for 2920

[2] The 'major' face of a Voronoi–Dirichlet polyhedron intersects a segment between contacting atoms.

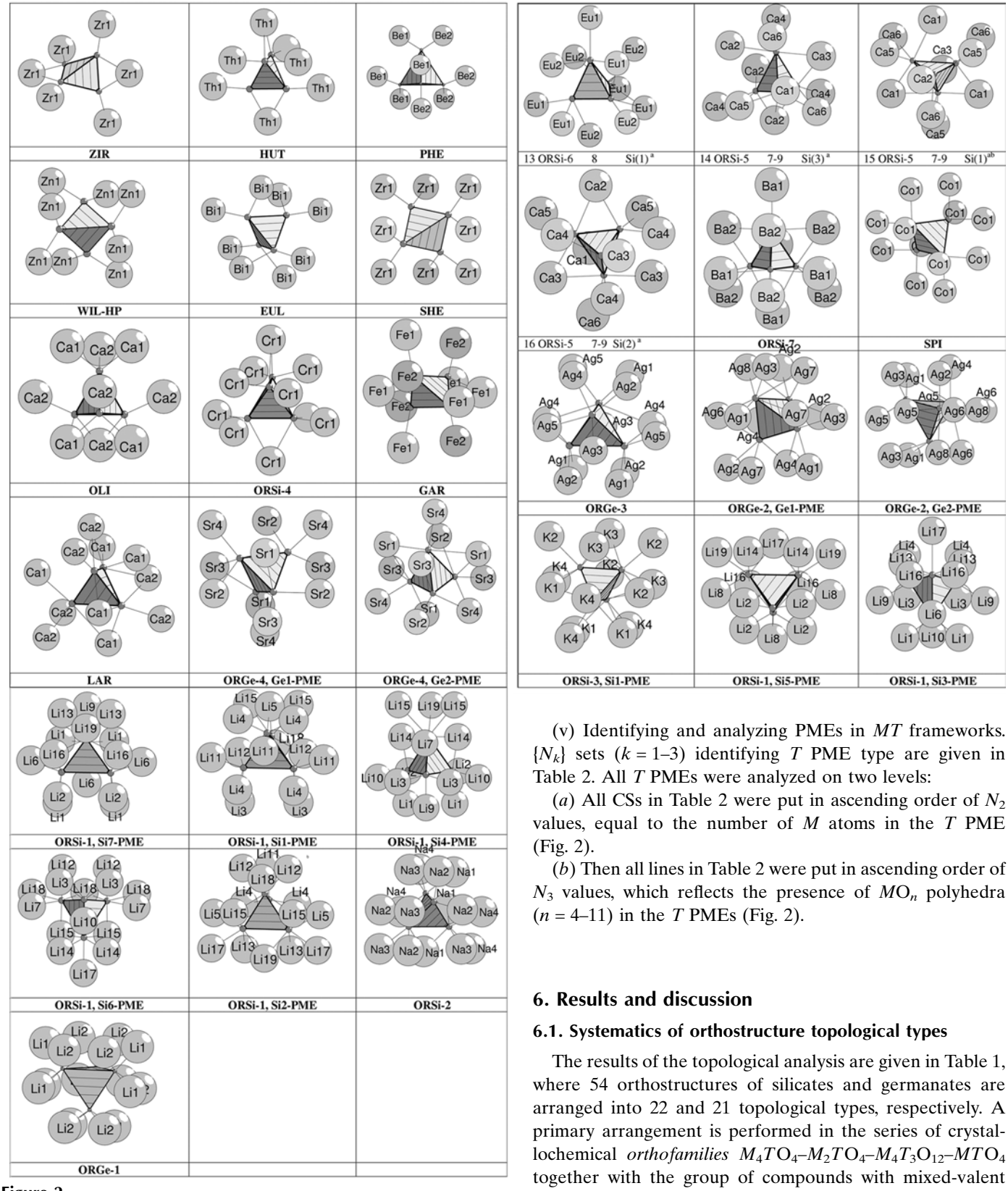

Figure 2
Topology of *T* PMEs.

framework A_yX_z compounds and 4658 topological types for 11570 framework $A_xB_yC_z$ compounds.

(v) Identifying and analyzing PMEs in *MT* frameworks. $\{N_k\}$ sets (k = 1–3) identifying *T* PME type are given in Table 2. All *T* PMEs were analyzed on two levels:

(*a*) All CSs in Table 2 were put in ascending order of N_2 values, equal to the number of *M* atoms in the *T* PME (Fig. 2).

(*b*) Then all lines in Table 2 were put in ascending order of N_3 values, which reflects the presence of MO_n polyhedra (n = 4–11) in the *T* PMEs (Fig. 2).

6. Results and discussion

6.1. Systematics of orthostructure topological types

The results of the topological analysis are given in Table 1, where 54 orthostructures of silicates and germanates are arranged into 22 and 21 topological types, respectively. A primary arrangement is performed in the series of crystallochemical *orthofamilies* M_4TO_4–M_2TO_4–$M_4T_3O_{12}$–MTO_4 together with the group of compounds with mixed-valent state of *M* atoms $[M(2+)_3M(3+)_2T_3O_{12}]$.

The topological features of orthosilicate and orthogermanate phases differ from each other: only eight topological types include both orthosilicates and orthogermanates; nine and four types, respectively, are

'pure'. In one case, the phases related to different structure types (spinel and Cu_2GeO_4) have the same topology and are united into the same topological family (SPI).

The number of orthosilicate structure types in Table 1 is nearly twice that in Bokij's (1998) systematics of minerals. Out of 17 orthosilicate types, nine types include minerals and eight types comprise synthetic phases only; out of 13 orthogermanate types, six types are found to be topologically analogous with silicate minerals, three types are topologically equivalent to synthetic silicate phases and only four types are unique by topology (Table 1).

The chemical composition of orthostructures is limited by the range $T{:}M$ = 1:1–1:4; the single exception is the metal-oxide phase Ag_5GeO_4 conditionally related to the orthofamily M_4TO_4. Orthostructures are stoichiometrically rather simple: the ratios 1:1 (three types), 1:2 (ten types) and 1:4 (six types) predominate; the topological types EUL and GAR correspond to the ratios 3:4 and 3:5, respectively. Obviously, M atoms in orthostructures can have an oxidation state (ξ_M) of no more than +4, otherwise extra O atoms appear that belong to no T tetrahedra. Analysis of all MTO ternary phases (585 silicates and 218 germanates) showed that they comprise no M atoms with $\xi_M > 4$ at all.

6.2. *T* PME and *M* PME overview

6.2.1. *T* PME topological features. Table 2 shows that the N_k indices vary starting from the second coordination sphere: ten different N_2 values in the range 6–16 correspond to 21 topological types; only N_2 = 13 is missing. The topological types are completely differentiated at the third coordination sphere (N_3 values vary in the range 21–49).

The 21 topological types comprise 31 T PMEs differing from each other by composition and topology: a unique set $\{N_1, N_2, N_3\}$ corresponds to each of the PMEs. Seventeen out of 21 topological types are unambiguously determined by the single T node topological properties. In the remaining four types, all crystallographically non-equivalent T nodes (2–7) are also topologically different. Thus, topological symmetry of T PMEs, so typical for the crystal structures of framework zirconosilicates and their analogs (Ilyushin & Blatov, 2002), is found for no orthophases in the MTO representation. The greatest topological similarity was revealed for Li_4SiO_4 where the pairs of Si2, Si6 and Si1, Si4 PMEs have identical CSs up to the sixth and fifth coordination sphere, respectively.

6.2.2. *M* PME topological features. The topological variety of M PMEs is much higher; the total number of topologically different M nodes is equal to 71. Although in many cases crystallographically non-equivalent M atoms have combinatorially similar coordination polyhedra (for instance, octahedra in OLI or tetrahedra in WIL-HP), corresponding M PMEs are rarely topologically symmetrical, unlike zirconosilicate M PMEs (such a situation occurs only in PHE, WIL-HP and ORGe-3). Moreover, the topological properties of M PMEs and T PMEs are the same in PHE and WIL-HP.

Two-thirds of the orthostructures are topologically determined by one or two types of M PMEs: in eight cases (ZIR, HUT, SHE, PHE, WIL-HP, SPI, EUL, ORSi-4) it is the single M PME type, in six cases (OLI, GAR, LAR, ORSi-7, LGE, Eu_2SiO_4) there are two M PME types. Other orthostructures are arranged as follows: four M PME types are found in three cases (ORGe-4, ORSi-2, ORSi-3); three, six, eight and 19 M PME types are revealed in ORGe-3, ORSi-5, ORGe-2 and LSI, respectively.

6.2.3. *T* PME symmetry. A rigid structure of atomic bonds in the central polyhedron of a T PME often causes its non-trivial local symmetry. Sixty-four crystallographically non-equivalent T atoms are arranged by symmetry of Wyckoff positions (given in parentheses) in 54 orthostructures as follows: 18 (m), 11 ($\bar{4}$), 6 ($\bar{4}3m$), 6 ($\bar{4}2m$), 3 (222), 1 ($mm2$). In merely 19 cases, T atoms occupy general positions. Only in the case of predominance of large M atoms (as in M_4TO_4 phases), or when large M polyhedra are strongly distorted, is the local structure of atomic bonds in a T tetrahedron completely dissymmetric.

The number of crystallographically different T atoms is always less than or equal to the number of crystallographic sorts of other atoms in orthostructures. Thus, in four low-symmetrical topological types of M_2TO_4 and M_4TO_4 families, the numbers of non-equivalent T atoms are equal to two (twice), three and seven; however, the numbers of non-equivalent M atoms are always much greater.

6.2.4. *M* PME symmetry. Out of the 71 crystallographically different M nodes, 14 nodes have the m point group; in three cases, M atoms are allocated on twofold axes. Seven cases are revealed of unique point symmetry: $\bar{4}2m$ for an M bisphenoid in zircon; $\bar{3}m$, $\bar{3}$, 3 and $\bar{1}$ for M octahedra in spinel, garnet, eulytite and olivine, respectively; $\bar{4}$ for the eight-vertex polyhedron in scheelite; and 222 for the M cube in garnet. In three cases, M polyhedra with different symmetry coexist in the same crystal structure: olivine ($\bar{1}$ and m), garnet (222 and $\bar{3}$) and Li_4SiO_4 (ten M polyhedra have the m point group, the remaining nine M polyhedra are allocated in general positions). In most cases (47), M polyhedra and corresponding M PMEs are dissymmetrical.

6.2.5. *T* PME polyhedral composition. As mentioned above, a typical distinction of T atoms is that the second coordination sphere is composed of only M atoms whereas an M PME can frame both T and M polyhedra. This feature, in particular, allows one to find all sterically possible T PMEs. The number of vertices (n) of MO_n polyhedra varies from four to ten, as a rule; n = 2 and 3 are found for only two Ag germanates (Table 2). The total number of M polyhedra in a T PME varies from 6 (for M eight-vertex polyhedra) to 16 (for M tetrahedra).

M polyhedra with even n are typical for homogeneous T PMEs: n = 4 (tetrahedra, three types of T PMEs), 6 (octahedra, four types) and 8 (two types). There are isolated instances with n = 9 (HUT) and 10 (ORSi-7). Ten orthostructure topological types comprise heterogeneous T PMEs where M atoms have different coordination numbers.

Let us consider the structural features of the nine homogeneous T PMEs composed of equivalent M polyhedra. These types are of special interest because almost all of them (eight

out of nine) possess baric and/or thermal polymorphism, to be analyzed in §6.4.

6.3. Features of *T* PME polyhedral self-assembly

6.3.1. Zircon topological family. In the zircon crystal structure, the *T* PME contains a minimum number (6) of *M* polyhedra. However, owing to the high *n* value, the total number of O atoms in the third coordination sphere is rather large ($N_3 = 36$) and corresponds to the average N_3 values in Table 2.

The *T* PME (Fig. 3) is coded as {O4, *M*6, O36} and contains six *M* bisphenoids forming two short chains three by three. The 3*M* chains have cross (tetrahedral) orientation; the central *M* polyhedra in the 3*M* chains are connected with the *T* tetrahedron by their edges.

6.3.2. Scheelite topological family. This topological family is more typical for germanates (Table 1). The numbers of *M* polyhedra and of peripheral O atoms in the *T* PME {O4, *M*8, O44} are maximum for homogeneous *T* PMEs. Only two orthophases (Ca_2SiO_4 and Ba_2SiO_4) have heterogeneous *T* clusters with greater N_3 values (46 and 49, respectively). MO_8 polyhedra are dissymmetric dodecahedra and surround the *T* tetrahedron as a bent eight-section ring (Fig. 4). Such a ring configuration explains the aforementioned maximum number of large *M* polyhedra in the *T* PME. The symmetry of the repeating ring fragment (marked by different hatching in Fig. 4), which contains a pair of *M* polyhedra connected with the central *T* tetrahedron, conforms to the point group $\bar{4}$.

6.3.3. Huttonite topological family. The coordination number of *M* atoms ($n = 9$) in the huttonite crystal structure is maximum for homogeneous *T* PMEs. Increasing *n* up to 9 is accompanied by decreasing the number of *M* polyhedra in the *T* PME to seven in comparison with eight *M* polyhedra ($n = 8$) in the scheelite *T* PME.

The *T* PME has the coding {O4, *M*7, O42}. All seven *M* polyhedra are united in an array where one can conditionally separate two groups as a 4*M* ring and a V-configured 3*M* chain. Both square 4*M* ring and 3*M* chain share an edge and a vertex with the central *T* tetrahedron (Fig. 5). The number of edge *M*–*T* contacts and their space location on the non-crossing *T* tetrahedron edges correspond to a similar configuration in the zircon crystal structure. Such a complex geometrical–topological structure of the *T* PME is stipulated by the absence of symmetrical relations between O atoms of the *T* tetrahedron.

6.3.4. Phenakite topological family. In the crystal structures of the phenakite-like compounds, chemically different cations have tetrahedral coordination and the same environment topologies (the same $\{N_k\}$ sets). The *T* PME is coded as {O4, *M*8, O21}; the central *T* tetrahedron is surrounded by eight *M* tetrahedra (Fig. 6). The number of *M* tetrahedra in the *T* PME is twice that in zeolite-like tetrahedral frameworks or SiO_2 phases, which confirms the doubling of *M* atoms in the phenakite chemical composition in comparison with tetrahedral aluminosilicates, for instance, with $NaAl^{[4]}SiO_4$, where Na atoms occupy voids in the tetrahedral framework.

The *T* PME local symmetry is *m*; the mirror plane passes through the central *T* atom and two *M* atoms of a diortho-group and divides the 6*M* ring into two sections (Fig. 6). In the

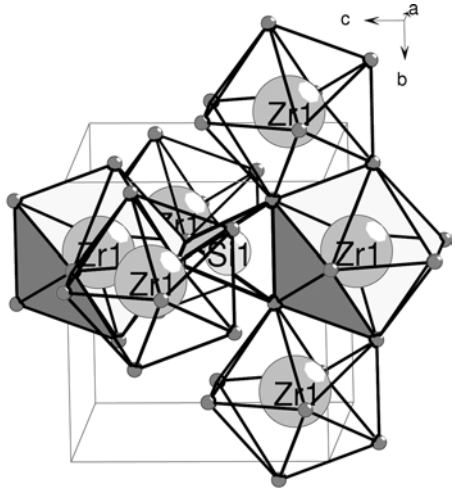

Figure 3
T PME in the zircon crystal structure.

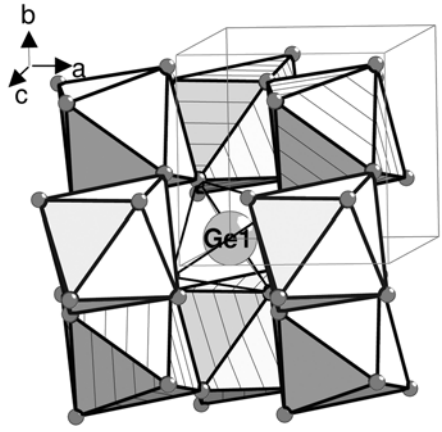

Figure 4
T PME in the scheelite crystal structure.

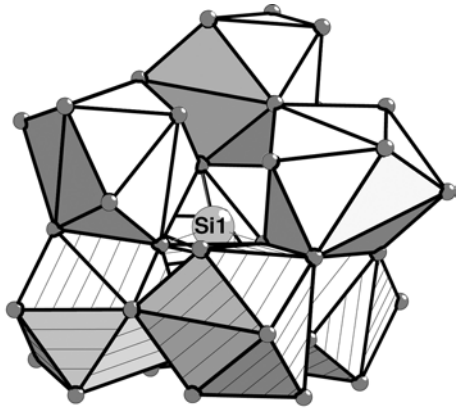

Figure 5
T PME in the huttonite crystal structure.

crystal structure, the *T* PME is dissymmetrical because all O atoms are crystallographically non-equivalent.

Three vertex *M*–*M* contacts are insufficient to connect all eight *M* tetrahedra into a chain, therefore three O atoms of the *T* PME unite six *M* tetrahedra into a ring; the two remaining *M* tetrahedra form an isolated diorthogroup (Fig. 6).

6.3.5. High-pressure willemite topological type. The high-pressure phase of Zn_2SiO_4 forming a separate topological type belongs to the family of tetrahedral crystal structures as phenakite, but the *T* PME has another composition: {O4, *M*8, O24}. As for PHE, the central tetrahedron in WIL-HP is surrounded by eight *M* tetrahedra (Fig. 7), but the number of O atoms in the third coordination sphere is greater and is maximum for N_2 and n (Table 2). Consequently, the *M* tetrahedra have no additional vertex contacts (Fig. 7) and the *T* PME is constructed invariantly: eight *M* tetrahedra are connected by O atoms of the central *T* tetrahedron into four isolated diorthogroups.

6.3.6. Eulytite topological family. The eulytite topological family, which has the coding {O4, *M*8, O32}, is the first example of crystal structures containing octahedral components in the *T* PME. Twelve O atoms of the third coordination sphere are bridge; eight of them are shared between eight *M* octahedra, and four O atoms are involved in edge contacts with *M* octahedra while forming short bent chains with four *M* octahedra in each chain (Fig. 8).

6.3.7. Olivine topological family. Olivine is a representative of the $A_2^{[6]}BX_4$ family. In comparison with EUL, a sharp increase of the number of *M* atoms in the compound composition from $M_{1.33}TO_4$ to M_2TO_4 results in an increase of the number of *M* octahedra in the *T* PME from eight to nine.

The *T* PME is coded as {O4, *M*9, O31}, so the nearest environment of the *T* tetrahedron consists of nine *M* octahedra. The *T* PME has *m* symmetry in the crystal structure, but the *T* PME itself (with no consideration of the next coordination spheres) has the point group 3*m*, which occurs only in the OLI topological family. The set of nine *M* octahedra can conditionally be divided into the three groups:

(i) three *M* octahedra are connected with each other and with the *T* tetrahedron by their edges;

(ii) three isolated *M* octahedra lie in the same plane as the *T* tetrahedron and share vertices with it;

(iii) the group of three *M* octahedra, translationally equivalent to the first group, is placed above the *T* tetrahedron, sharing with it one vertex, common to all three *M* octahedra (Fig. 9).

The crystal structures of the OLI family can be formed both at melt crystallization [Mg_2SiO_4 (Chukhrov, 1972)] and as a

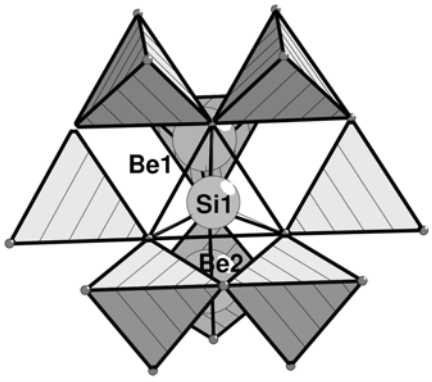

Figure 6
T PME in the phenakite crystal structure.

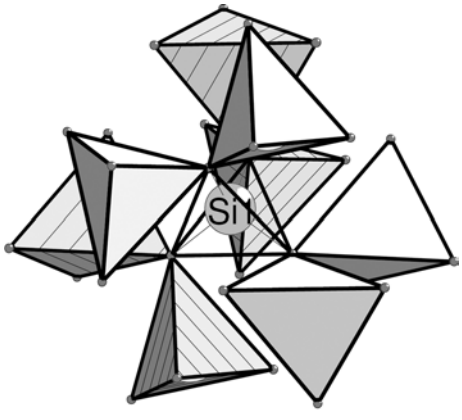

Figure 7
T PME in the high-pressure willemite crystal structure.

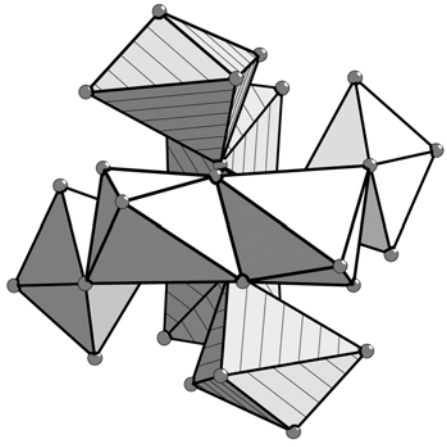

Figure 8
T PME in the eulytite crystal structure.

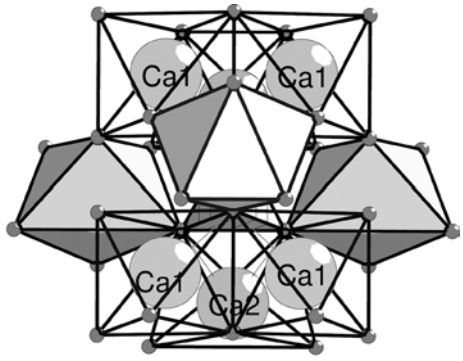

Figure 9
T PME in the olivine crystal structure.

result of a series of phase transitions. For instance, γ-Ca_2SiO_4 is the fifth (and last) phase that is stable at room temperature.

6.3.8. Cr_2SiO_4 topological family. The *T* PME in the topological family of synthetic-phase Cr_2SiO_4 is coded as {O4, *M*10, O32}. Thus, despite the olivine-like stoichiometric composition of Cr_2SiO_4, its *T* PME contains more *M* octahedra and its local symmetry (the point group 222) is unique for orthostructures.

The 10*M* group in the *T* PME is formed by two parallel 3*M* chains connected by two pairs of *M* octahedra. The central *M* octahedra of the 3*M* chains connect with the central *T* tetrahedron of the *T* PME by their edges; the remaining *M* octahedra share vertices with it (Fig. 10). Cr atoms are shifted from the centers of the *M* octahedra, probably owing to metal–metal bonds (Dollase *et al.*, 1994); the coordination polyhedra of Cd atoms in Cd_2SiO_4 and of Hg atoms in Hg_2GeO_4 have no such geometrical features.

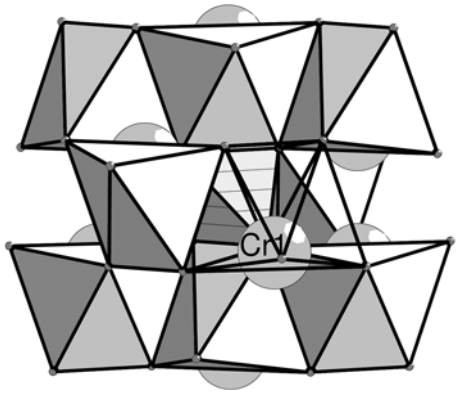

Figure 10
T PME in the Cr_2SiO_4 crystal structure.

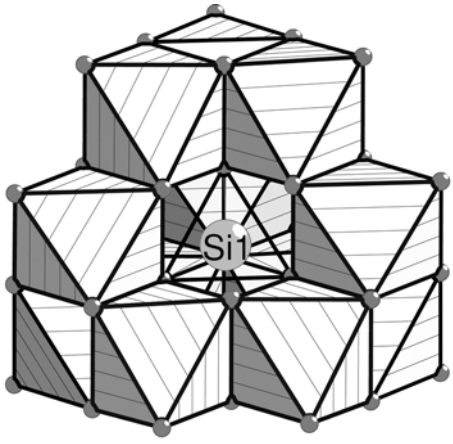

Figure 11
T PME in the spinel crystal structure.

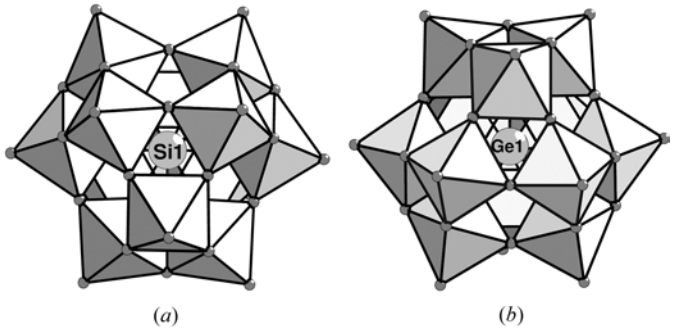

Figure 12
$TM_{12}O_{40}$ clusters: (*a*) *T* = Si; *M* = Mo; (*b*) *T* = Ge; *M* = Al.

6.3.9. Spinel topological family. Spinel *T* PME {O4, *M*12, O36} has the local symmetry $\bar{4}3m$; this is an example of a *T* PME with the highest symmetry. The spinel topological family is the third representative of the crystallochemical family $A_2^{[6]}BX_4$ considered here. In comparison with Cr_2SiO_4, the number of *M* octahedra in the spinel *T* PME increases from 10 to 12; this is the maximum possible N_2 for homogeneous *T* PMEs with an octahedral *M* component.

The high cubic symmetry of the spinel crystal structure determines rigidly the positions of *T* and *M* atoms in the unit cell; hence, the interatomic distances in *T* and *M* polyhedra are interdependent. The high concentration of *M* polyhedra in the *T* PME can destabilize the crystal structure owing to steric strains. The increased size of the central *T* tetrahedron in orthogermanates increases the size of the *T* PME as a whole and the *M*—*M* distances, which facilitates the formation of the Mg_2GeO_4 spinel-like crystal structure at normal pressure.

Spinel is characterized by a maximum N_2 value among all orthostructures with homogeneous *T* PMEs. This causes edge condensation of *M* octahedra, which form four equivalent groups of three octahedra allocated at four vertices of the central *T* tetrahedron (Fig. 11).

Note that two topologically different types of {O4, *M*12, O36} clusters are presently known, which exist as isolated particles $SiMo_{12}O_{40}$ and $GeAl_{12}O_{40}$ (Fig. 12*a*,*b*) in the crystal structures of $SiMo_{12}O_{40}(H_2O)_{13}$ [CC = 20683][3], $Na_4Mo_{12}GeO_{40}(H_2O)_8$ [CC = 1220] and $[GeO_4Al_{12}(OH)_{24}(H_2O)_{12}](SO_4)_4(H_2O)$ (Schonherr & Gorz, 1983). The first cluster is similar to a filled olivine *T* PME (there are three additional *M* octahedra at the *T* PME periphery), whereas the second is a full topological analog of spinel *T* PME.

Representatives of many of the topological families considered above are connected with each other by thermal or baric phase transitions accompanied by appropriate *T* PME reconstructions. The topological features of such phase transitions are considered below.

6.4. Topological classification of phase transitions in orthostructures

6.4.1. Baric phase transitions. *Zircon–scheelite transition*. The baric phase transition of $ZrSiO_4$ from ZIR (Mursic *et al.*, 1992) to SHE (Kusaba *et al.*, 1986) is interesting as the coordination numbers (*n*) of *M* atoms are constant while the number of *M* atoms increases in the *T* PME. The mechanism of structure reconstruction can be described in terms of the changing local environment of the *T* nodes. Since *n* is constant, the reconstruction has to be caused by changing the topology

[3] Hereinafter collection codes (CC) of compounds in the ICSD are given in brackets.

Table 3
Classification of phase transitions according to change of N_2 and N_3 indices.

Phase type before transition	Phase type after transition	Phase transition type† N_2	N_3
Baric transitions			
Zircon	Scheelite	+(6, 8)	+(36, 44)
Phenakite	Willemite-HP	=(8, 8)	+(21, 24)
Olivine	Spinel	+(9, 12)	+(31, 36)
Thermal transitions			
Zircon	Huttonite	+(6, 7)	+(36, 42)
Olivine	Larnite	+(9, 11)	+(31, 42)
Larnite	ORSi-5	=(11, 11)	+(42, 43.3‡)
ORSi-6	ORSi-7	=(11, 11)	+(43, 49)

† The type of phase transition ('=' or '+') and the values of N_2 and N_3 indices before and after the transition are given. ‡ Average value for three topologically different *T* PMEs is given.

of the binding *M* polyhedra, which is reflected by an increase in the number of O atoms in the third coordination sphere of the high-pressure phase, from 36 to 44 (Table 3).

Phenakite–willemite-HP transition. Both the willemite high-pressure phase (Marumo & Syono, 1971) and normal willemite (phenakite topological family; Simonov *et al.*, 1977) belong to the group of tetrahedral crystal structures; moreover, the number of *M* tetrahedra in the *T* PME is constant while the topological type changes. At the structure reconstruction, the number of O atoms in the third coordination sphere of the *T* atom increases up to 24 in the high-pressure phase (Table 3). The baric transition is accompanied by the depolymerization of 6*M* rings in the initial phase, namely, by its breaking into three isolated diorthogroups while the fourth diorthogroup, which existed before the transition, is not affected (Fig. 7).

Olivine–spinel transition. After the baric transition of olivine-like Ca_2SiO_4 (Kudoh & Takeda, 1986) to spinel topological type (Yamanaka *et al.*, 1998), both N_2 and N_3 indices increase (Table 3), reflecting significant reconstruction of the *T* PMEs (Figs. 9 and 11). Note that all efforts to perform such a transition for Mg_2SiO_4 are unsuccessful: the high-pressure β-Mg_2SiO_4 phase (Finger *et al.*, 1993) contains Si_2O_7 radicals and relates to the group of diorthosilicates. Bokij (1998) wrongly classified this phase as orthosilicate. Note that phase transitions with a change of Si-containing anion type are rather rare for silicates.

6.4.2. Thermal phase transitions. *Zircon–huttonite transition*. The high-temperature transition of $ThSiO_4$ from ZIR to HUT (Taylor & Ewing, 1978) is accompanied by an increase of N_2 from 6 to 7 and of *n* from 8 to 9. As a result, the number of *T* PME peripheral O atoms (N_3) increases from 36 to 42; this number is one of the largest values in Table 3. The aforesaid parameters differ from the baric zircon–scheelite transition where N_2 and N_3 values increase more significantly while *n* is unchanged.

Olivine–larnite transition. The thermal transition of Ca_2SiO_4 from OLI to LAR (Tsurumi *et al.*, 1994; Mumme *et al.*, 1996) results in a change of *T* PME coding from {O4, *M*9, O31} to {O4, *M*11, O42} and to an increase of *n* from 6 to 8–9 (Tables 2 and 3). Note that at the baric OLI–SPI transition the number of *M* polyhedra in the *T* PME increases even more (up to 12). Owing to the simultaneous increase of N_2 and *n*, the number of peripheral *T* PME O atoms increases from 31 to 42 and becomes one of the largest N_3 values in Table 3.

Larnite–ORSi-5 transition. A further increase of temperature stimulates the second phase transition of Ca_2SiO_4 (Mumme *et al.*, 1996), resulting in the appearance of three crystallographically and topologically different *T* PMEs (Table 2), while N_2 is unchanged and the average N_3 index increases slightly (Table 3).

ORSi-6–ORSi-7 transition. This transition is observed for Eu_2SiO_4 and it is accompanied by an increase of space symmetry from monoclinic (Felsche, 1971) to orthorhombic (Marchand *et al.*, 1978) and by a change of *T* PME coding from {O4, *M*11, O43} to {O4, *M*11, O49}. After the transition, the *T* PME local environment still has 11 Eu atoms with *n* values increased from 8 to 9–10. The high-temperature Eu_2SiO_4 phase shows the maximum N_3 value among all the *T* PMEs in Table 2.

6.4.3. Classification of phase transitions. The data obtained (Table 3) allow us to propose a two-level classification of the phase transitions considered above, which is based on the type of change of *T* PME composition (N_2 and N_3 values).

(i) The second coordination sphere of the *T* atom and the variation of the number of *M* atoms in the *T* PME (N_2) are considered.

(ii) The third coordination sphere of the *T* atom and the variation of the number of peripheral O atoms in the *T* PME (N_3) are considered.

On either of the two levels, three variants of change of topological index are theoretically possible, which correspond to three types of phase transitions: constant (type '='), decreasing (type '−') or increasing (type '+') index value. Thus, the mechanism of interpolyhedral *T–M* and *M–M* displacements at a phase transition can unambiguously be described at the local suprapolyhedral level by comparing geometrical–topological *T* PME features before and after the transition (Table 3).

Table 3 shows that baric and thermal phase transitions of orthostructures relate to the types '=' or '+', *i.e.* the number of *M* and O atoms in *T* PME can only remain constant or increase. Moreover, the same compound in a baric transition (zircon–scheelite or olivine–spinel) is characterized by a deeper structural reconstruction (greater increase of N_2 values) than in a thermal transition (zircon–huttonite or olivine–larnite). Note that at any phase transition an increase of N_2 index causes an increase of N_3 index; however, there are cases when N_2 stays constant [type '=' at classification level (i)] while N_3 increases [type '+' at classification level (ii)].

6.5. Orthostructure systematics and some regularities in *T* PME formation

Since in this study the *T* PME topological type is accepted as the basic criterion for orthostructure classification, it is

reasonable to group orthostructure topological types (Table 1) by the increase in N_2. Table 2 shows that such topological classification is directly connected with structural–chemical parameters, primarily with oxidation states of M atoms (ξ_M) whose decrease is accompanied by an increase of N_2 value. Actually, the topological families of zircon, huttonite and scheelite with $\xi_M = +4$ and of eulytite with $\xi_M = +3$ have small $N_2 = 6$–8. Conversely, large $N_2 = 14$–16 are typical for orthostructures with univalent cations. The increase of N_2 values results in an increase of the density of chemical bonds in the T PME; thus, in ORSi-1, ORSi-2 and ORGe-1, with maximum $N_2 = 15$–16 topological types, almost all O atoms are bridges between M atoms within the T PME. Additional factors resulting in more subtle differences in the T PME topological organization are the radius (r_M) and coordination number (n) of the M atom and the radius (r_T) of the T atom. Hence, we have separated five groups of topological types to be characterized by the following combinations of these parameters.

(i) Four topological families (ZIR, SHE, HUT and EUL) with $N_2 = 6$–8 and large $\xi_M = +3$, +4. They completely cover two crystallochemical orthofamilies MTO_4 and $M_4T_3O_{12}$. The high oxidation states of the M atoms cause small N_2 values, since a T PME with many M polyhedra would be unstable because of the strong mutual repulsion of the M cations.

(ii) Two topological types (PHE and WIL-HP) with $N_2 = 8$, small $n = 4$, small r_M and $\xi_M = +2$. In this group, small N_2 values are first caused by small n values and small sizes of the M polyhedra, which, together with the rather high oxidation state of the M atoms, hinder M tetrahedra from edge condensation.

(iii) Three topological families (OLI, ORSi-4 and SPI) with $N_2 = 9$–12, intermediate $n = 6$, intermediate r_M and $\xi_M = +2$. This group includes topological families where similar M polyhedra (M octahedra) connect differently with each other.

(iv) Five topological types (GAR, ORSi-5, LAR, ORSi-7, ORGe-4) with $N_2 = 10$ (GAR) and 11, coordination-mixed M PMEs ($n = 6$–10), intermediate and large r_M values. These topological types are primarily united by close N_2 values, despite having a variety of n values and types of coordination polyhedra. Obviously, $N_2 = 10$–11 conforms to an optimal number of bivalent M atoms in the nearest environment of the T tetrahedron.

(v) Six topological types (ORGe-1, ORGe-2, ORGe-3, ORSi-1, ORSi-2, ORSi-3) with $N_2 = 14$–16 and $\xi_M = +1$. This group of orthostructures with univalent cations is characterized by having the maximum number of M atoms in the chemical composition. N_2 values are also maximum, and a clear tendency is observed of increasing this value while decreasing r_M and increasing r_T in the series K^+–Ag^+–Na^+–Li^+. Thus, Li_4GeO_4 has the maximum $N_2 = 16$, where the ratio r_T/r_M is also maximum, whereas K_4SiO_4 (which has minimum $N_2 = 14$ along with Ag germanates) is characterized by a minimum r_T/r_M ratio. In most topological types, the T PMEs are dissymmetrical except for the Li phases: in the crystal structures of Li_4GeO_4 and Li_4SiO_4, the T PMEs have local symmetry $mm2$ and m, respectively. All compounds of this group have shortened $M—M$ contacts (in comparison with metal phases) with rather high maximum $\Omega(M—M)$ values (Table 4). This is due to the high cation concentration and indicates that significant intercationic interactions exist. In Ag orthogermanates, $M—M$ distances practically coincide with such distances in metallic silver.

Table 4
Characteristics of metal–metal contacts in orthostructures and simple substances.

M atom	$R_{min}(M–M)$ in metal (Å)	$R_{min}(M–M)$ in orthostructures (Å)	$\Omega_{max}(M–M)$ in orthostructures (%)
Li	3.04	2.30	8.8
Na	3.72	2.86	6.9
K	4.54	3.15	7.9
Ag	2.89	2.74	11.7

The aforementioned factors influencing T PME composition and topology allow us to propose the following scheme of T PME formation in orthostructures.

(i) The T PME is based on a T tetrahedron (SiO_4 or GeO_4) whose geometry slightly changes from compound to compound and primarily depends on the size of the T atom. Geometrical inflexibility of the T tetrahedron allows it to be considered as a template, as a matrix on which the suprapolyhedral structure fragment is assembled.

(ii) The T-tetrahedron topology (presence of four condensation centers) and its fixed size determine the maximum possible number of M polyhedra in the T PME [N_2(max)]. The data obtained also show that the variants of face-to-face condensation of T and M polyhedra (in addition to vertex and edge-binding constructions) are extremely rare in orthostructures (Table 2). This results in a decrease of N_2(max).

(iii) The number of M polyhedra to be condensed on the surface of the T template is additionally restricted by their sizes and their capability for mutual vertex, edge or face-to-face condensation. At present, the prediction of a strict N_2 value in a given crystal structure seems to be impossible; however, the N_2 dependencies on the size of the M polyhedron and the charge of the M cation allow one to forecast the range of possible changes for this index. To do this, one should relate the orthostructure to one of the aforementioned five groups. Apparently, the value $N_2 = 16$ found in ORGe-1 is maximum for orthostructures at normal pressure because this case realizes the most favorable combination of factors for condensing M polyhedra (the largest size of T atom, the smallest size of M atom and the smallest charge of M cation).

Above, the results of orthostructure classification were considered within the local suprapolyhedral approach. At the same time, the methodology of this approach, which uses the topological models of the 'reduced' graph of crystal structure and a suprapolyhedral invariant as a 'building block' of such a graph, can be easily extended to a description of crystal structure global topology. In the next section, we will show how the 'global' approach to the analysis of orthostructures when they are considered as packings of finite structure units (atoms, polyhedra or suprapolyhedral invariants) can supplement the local suprapolyhedral approach. In a sense, the

Table 5
The topological correspondences between the orthostructures $M_y(TO_4)_z$ and the binary compounds A_yX_z according to the scheme $M \leftrightarrow X$; $TO_4 \leftrightarrow A$.

Orthostructure topological type	A_yX_z compound	Isomorphic atomic substructures	Coordination number†	N_1	N_2	N_3
LAR, ORSi-5, ORSi-6, ORSi-7, ORGe-4‡	BaF_2	*M*1; *F*1	5	32	158	392
		*M*2; *F*2	6	38	172	400
		TO_4; Ba	11	20	86	200
ORSi-4	$TiSi_2$	*M*; Si	5	30	128	288
		TO_4; Ti	10	18	66	146
SPI	NdS_2	*M*; S	6	36	186	462
		TO_4; Nd	12	28	118	266
EUL	Th_3P4	Bi; P	6	26	113	293
		SiO_4; Th	8	20	86	224

† Coordination numbers of atoms or TO_4 anions in corresponding crystal structure representation. In particular, coordination number of a metal atom *M* in an $M_y(TO_4)_z$ compound is equal to the number of TO_4 groups, not O atoms, connected with *M*. ‡ Topological supersymmetry is found in the following topological types: ORSi-5: *M*1 = Ca1–3, *M*2 = Ca4–6, *T* = Si1–3; and ORGe-4: *M*1 = Sr1,2, *M*2 = Sr3,4, *T* = Ge1,2.

change from 'local' to 'global' approach is related to Bragg's scheme where 'local' condensation of tetrahedra and octahedra can result in 'global' close packing of O atoms. However, graph-theoretical methods allow one to enrich and to generalize Bragg's approach and to confine more objectively the area of its applicability to orthostructures.

6.6. Global topology of orthostructures

6.6.1. Relationships with binary compounds. *'Gray' isomorphism*. The results obtained show the relationships of orthostructures and binary compounds on two levels of topological similarity. The first higher level appears as 'gray' isomorphism of 'reduced' graphs (Ilyushin & Blatov, 2002), *i.e.* as topological equivalence of at least two atomic chemical sorts in a crystal structure. With 'gray' isomorphism, chemically more complex orthostructures ($R = 3$) correspond to binary compounds ($R = 2$) as chemically ordered superstructures. This type of isomorphism was found for three pairs of topological types of binary A_yX_z and $M_y(TO_4)_z$ compounds:

(i) $C_3^{[4]}N_4$ [CC = 41950] and $Be_2^{[4]}Si^{[4]}O_4$ (PHE);

(ii) $Fe_3O_4 = [Fe^{[6]}(2+)Fe^{[6]}(3+)]Fe^{[4]}(3+)_2O_4$ and $Co_2^{[6]}Si^{[4]}O_4$ (SPI);

(iii) $Tl_2Cl_4 = Tl^{[8]}(+)Tl^{[4]}(3+)Cl_4$ [CC = 4031] and $Zr^{[8]}Ge^{[4]}O_4$ (SHE).

Note that, among the three orthostructure topological types, *M* and *T* atoms have the same topology only in PHE, where their CSs coincide with the CSs of C atoms in C_3N_4 while the O atoms correspond to the two crystallographically non-equivalent N atoms. In two other topological types, the anionic arrays are topologically the same while different crystallographic sorts of cations in the binary compounds correspond to *M* and *T* atoms in the orthostructures. As a result, five orthosilicates and nine orthogermanates were found to be isotypic to binary compounds on this level of topological similarity.

Partial isotypism. The second level is represented by partial isotypism (Blatov, 2000) of A_yX_z and $M_y(TO_4)_z$ compounds and can be described by the following correspondences: $M \leftrightarrow A$ (or *X*); $TO_4 \leftrightarrow X$ (or *A*). With partial isotypism, the stoichiometric and topological similarity of an orthostructure and a binary compound is reached by contracting O atoms to *T* atoms and representing *T* tetrahedra as structureless particles. All four cases of such topological similarity found by the *IsoTest* program are given in Table 5 and discussed in detail below.

(i) All topological types of orthostructures with $N_2 = 11$ are similar to the BaF_2 orthorhombic high-pressure phase [CC = 41651, Ni_2In structure type (Leger *et al.*, 1995)] where the coordination number of Ba atoms is also equal to 11 (Figs. 13*a* and 13*b*).

This fact indicates the mutual similarity of all topological types $N_2 = 11$ and explains their mutual phase transitions as considered above. The topological supersymmetry of *T* and *M* nodes, which appears after contracting O atoms to *T* atoms, is observed in all the topological types. Thus, their topological differences (Table 2) are caused only by various orientations of *T* tetrahedra relative to *M* atoms, which result in different *n* values; all the crystal structures can be topologically transformed to each other by appropriate rotations of *T* tetrahedra. Note that in a recent study (Vegas & Jansen, 2002) LAR was related to the cotunnite ($PbCl_2$) structure type, which is topologically close to, but not equal to, BaF_2 (in cotunnite $n_{Pb} = 9$ whereas in BaF_2 $n_{Ba} = 11$).

(ii) The Cr_2SiO_4 topological family is topologically and geometrically similar to the family of disilicides $CrSi_2$ [CC = 16836], $TiSi_2$ [CC = 1089], $NbSi_2$ [CC = 16502] and $TaSi_2$ [CC = 43596]; the oppositely charged ionic substructures in these families are isotypic (Figs. 14*a* and 14*b*).

(iii) The SPI topological family is isotypic with NdS_2 [CC = 76604]; an 'inversion' in the similarity of ionic arrays is also observed in this case (Figs. 15*a* and 15*b*).

(iv) The EUL topological family show topological and geometrical relationships with the Th_3P_4 structure type with the 'inverted' correspondences $Bi^{3+} \leftrightarrow P^{3-}$ and $TO_4^{4-} \leftrightarrow Th^{4+}$ (Figs. 16*a* and 16*b*).

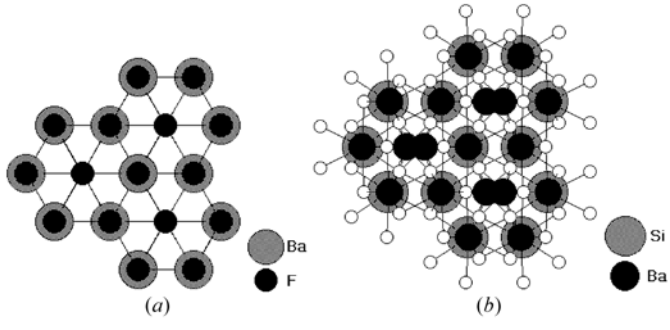

Figure 13
Crystal structure projections of (*a*) BaF_2 to (100) and (*b*) Ba_2SiO_4 to (001).

Table 6
Oxygen-containing representatives of the ZIR, HUT and SHE topological families.

ξ_M:ξ_T	Zircon	Huttonite	Scheelite
1:7			$NaIO_4$ $NaReO_4$ KIO_4 $KReO_4$ $KRuO_4$ $KTcO_4$ $RbIO_4$ $RbReO_4$ $CsBrO_4$ $AgReO_4$
2:6	$CaCrO_4$ $SrMoO_4$ $SrWO_4$	$PbCrO_4$ $PbSeO_4$ $SrSeO_4$ $SrCrO_4$	$CaWO_4$ $CaMoO_4$ $PbMoO_4$ $PbWO_4$ $CdMoO_4$
3:5	$BiVO_4$ $DyVO_4$ $DyPO_4$ $DyAsO_4$ $DyCrO_4$	$LaPO_4$ $LaCrO_4$ $CePO_4$ $PrPO_4$ $NdPO_4$ $GdPO_4$ $SmPO_4$	$ErVO_4$ $BiVO_4$ $BiAsO_4$
5:3	$NbBO_4$ $TaBO_4$		

Thus, on this level, seven topological types of orthosilicates (12 phases) and four topological types of orthogermanates (seven phases) have topological analogs among four topological types of binary compounds. A common property of all these relationships is the aforementioned 'inverted' topological correspondence of cations and anions in the orthostructures with ionic substructures of binary phases.

6.6.2. Relationships with ternary compounds. We have found the following relationships between orthostructures and ternary compounds:

(i) The Na_4SiO_4 topological family also includes Na_4CrO_4 [CC = 62676], K_4SnO_4 [CC = 158] and K_4PbO_4 [CC = 37268];

(ii) The Li_4GeO_4 topological type includes Li_4PbO_4 [CC = 38350] and Li_4TiO_4 [CC = 75164];

(iii) The PHE topological family contains Li_2BeF_4 [CC = 72423], Li_2CrO_4 [CC = 1972] and Li_2WO_4 [CC = 15395];

(iv) The Cr_2SiO_4 topological family comprises Ag_2SO_4 [CC = 27655], Na_2SO_4 [CC = 2895] and Na_2SeO_4 [CC = 16042];

(v) The LAR topological type is extended with Ba_2TiO_4 [CC = 2625];

(vi) The K_4SiO_4 topological family additionally comprises Cs_4SnO_4 [CC = 65970].

Moreover, numerous topological analogs were found for the orthostructures related to the topological families OLI, SPI, ORSi-7, SHE, HUT and ZIR; the number of phases for the first two M_2TO_4 families reaches three hundred. Some instances of relationships between the last three MTO_4 families and oxide compounds are given in Table 6.

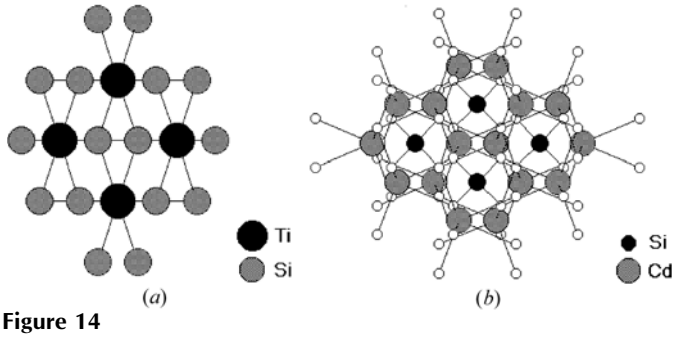

Figure 14
Crystal structure projections of (*a*) $TiSi_2$ to (010) and (*b*) Cd_2SiO_4 to (010).

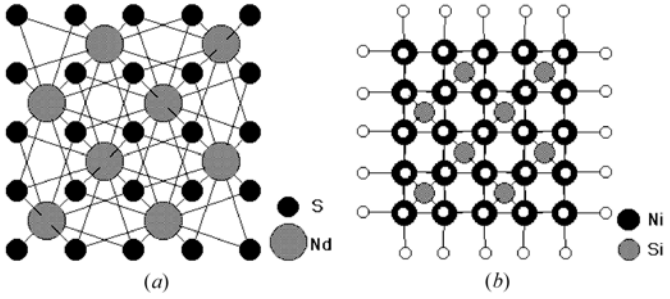

Figure 15
Crystal structure projections of (*a*) NdS_2 to (001) and (*b*) Co_2SiO4 (SPI) to (001).

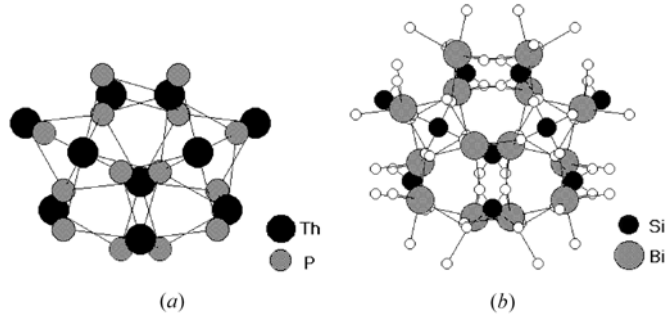

Figure 16
Crystal structure projections of (*a*) Th_3P_4 to (001) and (*b*) $Bi_4(SiO_4)_3$ to (001).

Note that in five topological types (SPI, ZIR, SHE, WIL-HP and ORSi-4) *T* substructure connectedness corresponds to the topology of a diamond-like net, *i.e.* in all five cases the *T* PMEs considered as structureless particles are connected in the same way. The CS identifying this type of three-dimensional net is equal to {4, 12, 24, 42, 64, 92, . . . }.

7. Conclusions: the suprapolyhedral approach and Bragg's scheme

The classification scheme for orthostructures based on the concept of suprapolyhedral invariants allows one to resolve the principal problems of Bragg's scheme listed in §1.

7.1. The problem of hierarchy and unambiguity

The concept of a suprapolyhedral invariant as a polyhedral microensemble of the *n*th sublevel gives one an opportunity to characterize unambiguously any local domain of crystal structure by a set of indices as a coordination sequence. Arranging PME coordination sequences for various substances in ascending order of corresponding N_k values determines the *hierarchy* of such a classification. Owing to this hierarchy, the result of classification of a new orthophase can be of two kinds. In the first case, the set of indices for this orthophase could coincide with the existing set; then the orthophase is to be related to the appropriate topological family; otherwise, the orthophase is to form a new topological type with hierarchically determined position in the systematics. In the case of orthosilicates and orthogermanates, only PME-1s of *T* atoms are sufficient to arrange the compounds unambiguously into topological types and families. As shown above, such *T* PME parameters as the numbers of *M* atoms (N_2) and peripheral O atoms (N_3) and the type of *M* polyhedra are crystallochemically important. However in other classes of substances with high chemical complexity [as in zirconosilicates where $R = 4$–11 (Ilyushin & Blatov, 2002)], a deeper comparison of coordination sequences can be required, and in the most complex cases one should consider PMEs of other cations.

7.2. The problem of comparison

In this study, the crystal structures of orthosilicates and their analogs with minimum $R = 3$ were studied. However, oxo-orthostructures and more complex orthostructures with $R > 3$ can be classified in the same way. Note that among the compounds considered two topological families already have superstructural analogs in the orthosilicates with $R = 4$: OLI ($R = 3$) with monticellite ($MgCaSiO_4$, $R = 4$), and GAR ($R = 3$) with $Ca_3Fe_2(SiO_4)_3$ ($R = 4$). Recently the problem of comparing crystal structures with different chemical-complexity ranks was studied by Ilyushin & Blatov (2002).

7.3. The problem of completeness

We have considered all known crystal structures of simple orthosilicates and their analogs, including the orthostructures with alkali and alkaline-earth atoms, to be topologically rather complex, irrespective of their formation conditions (as minerals or synthetic phases; at low or high temperature or pressure).

7.4. The problem of exceptions

In the classification proposed, all structure components are considered as structure-forming along with TO_4 tetrahedra. While classifying, the geometrical model of a given crystal structure is substituted with its topological type unambiguously determined by a set of coordination sequences; the crystallochemical properties of all atoms in the crystal structure are characterized by appropriate 'reduced' graphs. For instance, Cu_2GeO_4 was related to the SPI topological family (Table 1) despite essential differences in their crystallochemical data (space groups, Wyckoff indices, geometrical properties of *M* polyhedra). Moreover, in the analysis of crystal structures no *a priori* criteria are used for excluding cations from the group of *M* atoms and giving them the role of silicon understudies as often takes place for Be and Zn atoms.

The classification scheme proposed differentiates the largest parts in Bragg's systematics. It first selects the subsets with the same chemical complexity rank from the set of crystal structures to be classified. Then the crystal structures are arranged in ascending order of their crystallochemical complexity, taking into account the number and types of *M* polyhedra that form a local domain of a crystal structure (suprapolyhedral invariant). Switching from Bragg's PSUs (tetrahedra and octahedra) to suprapolyhedral clusters and using graphs for their representation is in fact the synthesis and further development of Pauling's and Wells's ortho-structure models.

This work was financially supported by the Russian Foundation for Basic Research (project No. 02-02-16861).

References

Belov, N. V. (1965). *Crystal Chemistry of Large Cation Silicates.* New York: Consultant Bureau.

Blatov, V. A. (2000). *Acta Cryst.* A**56**, 178–188.

Blatov, V. A. & Serezhkin, V. N. (2000). *Russ. J. Inorg. Chem. Suppl.* pp. S105–S220.

Blatov, V. A., Shevchenko, A. P. & Serezhkin, V. N. (2000). *J. Appl. Cryst.* **33**, 1193.

Bokij, G. B. (1984). *Dokl. Akad. Nauk.* **274**, 1210–1214.

Bokij, G. B. (1998). *Sytematics of Natural Silicates.* Moscow: VINITI.

Bragg, W. L. (1930). *Z. Kristallogr.* **74**, 237–305.

Bragg, W. L. & Claringbull, G. F. (1965). *Crystal Structure of Minerals.* London: Bell and Sons.

Brunner, G. O. & Laves, F. (1971). *Wiss. Z. Techn. Univ. Dresden*, **20**, 387–390.

Chukhrov, F. V. (1972). Editor. *Minerals: Handbook*, Vol. I. Moscow: Nauka. (In Russian.)

Dollase, W. A., Seifert, F. & O'Neill, H. S. C. (1994). *Phys. Chem. Miner.* **21**, 104–109.

Felsche, J. (1971). *Naturwissenschaften,* **58**, 218–219.

Finger, L. W., Hazen, R. M., Zhang, J., Ko, J. & Navrotsky, A. (1993). *Phys. Chem. Mineral.* **19**, 361–368.

Grice, J. D., Burns, P. C. & Hawthorne, F. C. (1999). *Can. Mineral.* **37**, 731–762.

Grosse-Kunstleve, R. W., Brunner, G. O. & Sloane, N. J. A. (1996). *Acta Cryst.* A**52**, 879–889.

Hassel, O. (1934). *Kristallchemie.* Dresden: Verlag von Theodor Steinkopff.

Ilyushin, G. D. & Blatov, V. A. (2002). *Acta Cryst.* B**58**, 198–218.

Ilyushin, G. D. & Demianets, L. N. (1989). *Germanates of Four-Valent Metals.* Moscow: VINITI. (In Russian.)

Ilyushin, G. D. & Demianets, L. N. (2001). *Crystallogr. Rep.* **46**, 801–809.

Ilyushin, G. D. & Demianets, L. N. (2002). *Structural Studies of Crystals.*, pp. 82–169. Moscow: Nauka.

Kostov, I. (1971). *Sov. Phys. Crystallogr.* **16**, 1220–1224.

Kudoh, Y. & Takeda, H. (1986). *Physica B and C*, **139**, 333–336.
Kusaba, K., Yagi, T., Kikuchi, M. & Syono, Y. (1986). *J. Phys. Chem. Solids*, **47**, 675–679.
Leger, J. M., Haines, J., Atouf, A., Schulto, O. & Hull, S. (1995). *Phys. Rev. B*, **52**, 13247–13256.
Liebau, F. (1956). *Phys. Chem.* **206**, 73–92.
Liebau, F. (1985). *Structural Chemistry of Silicates: Structure, Bonding and Classification.* Berlin: Springer.
Machatschki, F. C. (1928). *Zentralbl. Mineral. Geol. Palaeontol. Abt. A*, pp. 97–104.
Marchand, R., L'Haridon, P. & Laurent, Y. (1978). *J. Solid State Chem.* **24**, 71–76.
Marumo, F. & Syono, Y. (1971). *Acta Cryst.* B**27**, 1868–1870.
Meier, W. M. & Moeck, H. J. (1979). *J. Solid State Chem.* **27**, 349–355.
Meier, W. M., Olson, D. H. & Baerlocher, C. (1996). Editors. *Atlas of Zeolite Structure Types*, 4th ed. Amsterdam: Elsevier.
Moore, P. B. (1984). *Phosphate Minerals*, edited by J. O. Niagru & P. B. Moore, pp. 155–170. Berlin: Springer-Verlag.
Mumme, W., Cranswick, L. & Chakoumakos, B. (1996). *Neues Jahrb. Mineral. Abh.* **170**, 171–188.
Mursic, Z., Vogt, T., Boysen, H. & Frey, F. (1992). *J. Appl. Cryst.* **25**, 519–523.
O'Keeffe, M. (1995). *Acta Cryst.* A**51**, 916–920.
Puschcharovskii, Yu. D. (1986). *Structural Mineralogy of Silicates and Their Synthetic Analogs.* Moscow: Nedra. (In Russian.)
Schiebold, E. (1932). *Naturwissenschaften*, **11**, 352–434.
Schiebold, E. (1933). *Naturwissenschaften*, **12**, 219–296.
Schonherr, S. & Gorz, H. (1983). *Z. Anorg. Allg. Chem.* **503**, 37–42.
Simonov, M. A., Sandomirskii, P. A., Egorov-Tismenko, Y. K. & Belov, N. V. (1977). *Dokl. Akad. Nauk.* **237**, 581–588.
Smith, J. V. (1988). *Chem. Rev.* **88**, 149–182.
Stixrude, L. & Bukowinski, M. S. T. (1990). *Am. Mineral.* **75**, 1159–1169.
Taylor, M. & Ewing, R. C. (1978). *Acta Cryst.* B**34**, 1074–1079.
Tsurumi, T., Hirano, Y., Kato, H., Kamiya, T. & Daimon, M. (1994). *Ceram. Trans.* **40**, 19–25.
Vegas, A. & Jansen, M. (2002). *Acta Cryst.* B**58**, 38–51.
Wells, A. F. (1977). *Three-Dimensional Nets and Polyhedra.* New York: Interscience.
Wells, A. F. (1985). *Structural Inorganic Chemistry.* Oxford: Clarendon Press.
Yamanaka, T., Tobe, H., Shimazu, T., Nakatsuka, A., Dobuchi, Y., Ohtaka, O. & Nagai, T. (1998). *Geophys. Monogr.* **101**, 451–459.
Zoltai, T. (1960). *Am. Mineral.* **45**, 960–973.